

Particle Capture Efficiency in a Multi-Wire Model for High Gradient Magnetic Separation

Almut Eisenträger,¹ Dominic Vella,¹ and Ian M. Griffiths^{1, a)}

Mathematical Institute, University of Oxford, Radcliffe Observatory Quarter, Woodstock Road, Oxford, OX2 6GG, United Kingdom

(Dated: 17 September 2018)

High gradient magnetic separation (HGMS) is an efficient way to remove magnetic and paramagnetic particles, such as heavy metals, from waste water. As the suspension flows through a magnetized filter mesh, high magnetic gradients around the wires attract and capture the particles, removing them from the fluid. We model such a system by considering the motion of a paramagnetic tracer particle through a periodic array of magnetized cylinders. We show that there is a critical *Mason number* (ratio of viscous to magnetic forces) below which the particle is captured irrespective of its initial position in the array. Above this threshold, particle capture is only partially successful and depends on the particle's entry position. We determine the relationship between the critical Mason number and the system geometry using numerical and asymptotic calculations. If a capture efficiency below 100% is sufficient, our results demonstrate how operating the HGMS system above the critical Mason number but with multiple separation cycles may increase efficiency.

PACS numbers: 41.20Gz, 47.57.J-, 47.85.M-

Various applications require efficient removal of magnetic and paramagnetic particles from a carrier fluid, such as waste water treatment, food processing and microfluidics.^{1–5} In high gradient magnetic separation (HGMS), a suspension flows through a filter made of magnetized material, such as regular mesh grids or randomly packed material (steel wool) in the field of a strong electromagnet.⁶ The particles are deflected by magnetic forces due to the strong magnetic field gradients between the filter wires which enables particle capture within the filter. Despite these techniques remaining effectively unchanged since the 1970s,^{7,8} several theoretical questions remain unanswered.

The wire volume fraction in a typical HGMS system (2–15%) is well below what would be necessary for mechanical filtration. Nevertheless, the magnetic and hydrodynamic interactions between wires can play an important role in the trajectory of contaminant particles and whether they are captured. However, many previous attempts to model HGMS systems focus on the ability of a single wire to capture a single particle^{8–11} or to retain large numbers in the late stages of filtration.^{12–14} To model the effects of many wires, single-wire results are often superposed^{15,16} or particular geometries and parameter values are studied.^{3,17–19} These studies reveal that for potential flow within a periodic square lattice of cylinders, particles may escape filtration if they enter in a narrow escape trajectory whose width depends on the geometry, strength of magnetic interactions and viscous drag. In this Letter we focus on providing a complete understanding of this dependence, focusing in particular on the role of the packing density of the wires, which has not been systematically considered before, and how filtration efficiency can be maximized.

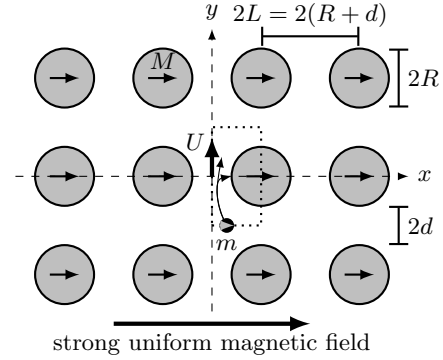


FIG. 1. Cylinder array and particle in Setup A (top view). The dotted box indicates the computational domain.

As a simplified model for the filter material, here we consider a large square array of long parallel cylinders of radius R with a constant magnetization perpendicular to their axes (Fig. 1). The magnetic dipole moment of the particle is constant and kept aligned with the magnetization of the cylinders by the action of a strong, uniform outer magnetic field. The smallest distance between cylinders in the x - and y -direction is denoted by $2d$, so that the period of the array in both directions is $2L = 2(R + d)$. Using symmetry across the y -axis, we may reduce the computational domain to half the periodic cell, (Fig. 1). We assume that the filtrate is a dilute suspension of magnetic particles. This allows us to neglect interactions between particles and focus on a single spherical magnetic particle moving through this cylinder array, carried by a fluid flow and deflected by the magnetic force exerted by the magnetic field of the cylinders. This model captures the important physics of the system and represents a worst case scenario, since higher particle concentrations would cause chains to form that would be

^{a)}ian.griffiths@maths.ox.ac.uk

captured more easily.²⁰

We consider two different setups. In Setup A, the magnetization of the cylinders and the particle are perpendicular to the flow direction (Fig. 1). In Setup B, both magnetizations are parallel to the flow direction. For a given setup and operating conditions, we are interested in whether a particle entering the computational domain at the inlet with $(x_p(0), y_p(0)) = (x_0, -L)$ can escape, that is, leave the domain at some $(x_p(t), y_p(t)) = (x_p(t), L)$, or whether its trajectory intersects the cylinder, in which case we say it has been captured.

For the calculations, we make the following assumptions. (a) The cylinders are infinitely long and the flow field is planar, *i.e.*, two-dimensional. (b) The cylinder array is infinite, thus both the flow field and the magnetic field can be considered to be periodic. (c) The flow is steady and laminar. (d) The particle diameter, $2a$, is small compared to the smallest distance between cylinders, $2d$, that is, $a/d \ll 1$, and so the particle does not disturb the flow field.

In practical applications, the operating Reynolds number ranges from 10^{-4} (*e.g.*, in food processing) to several hundreds (*e.g.*, in waste water treatment).^{3,16} Here we are concerned with full particle capture, which can be achieved either by increasing the strength of the magnetization or by decreasing the flow rate. Since the latter is more feasible in most cases, we assume we are in the lower Reynolds number range and model the fluid flow as Stokes flow. However, the following analysis might readily be extended to potential flow or the full Navier–Stokes equations.

Neglecting inertial terms, the net force on the particle must be zero, *i.e.*, the magnetic force, \mathbf{F}_m , and the viscous drag force (Stokes drag) must balance, giving

$$6\pi\eta a [\mathbf{u}(\mathbf{x}_p) - \dot{\mathbf{x}}_p] + \mathbf{F}_m = 0, \quad (1)$$

with η the fluid viscosity and \mathbf{x}_p the particle position. The dot $\dot{}$ denotes differentiation with respect to time. The force exerted on a particle due to a single magnetic cylinder is given by²¹

$$\mathbf{F}_{m, \text{single}} = \mp \frac{\mu_0 m M}{R} \left(\frac{R}{r} \right)^3 \begin{pmatrix} \cos 3\theta \\ \sin 3\theta \end{pmatrix}, \quad (2)$$

where \mp corresponds to Setup A/B, respectively, μ_0 is the permeability of free space, M the magnetization of the cylinders, m the magnetic dipole moment of the particle, and r and θ the plane-polar coordinates centered at the cylinder midpoint. The total magnetic force on a particle is the sum of the contributions from all cylinders in the array.

Upon nondimensionalizing the system, we find that the behavior of the particle is governed only by its initial position and the so-called Mason number, which measures the strength of the viscous forces compared with the magnetic forces in the system,^{21,22}

$$\text{Mn} = \pm \frac{6\pi\eta a R U}{\mu_0 m M} \quad (3)$$

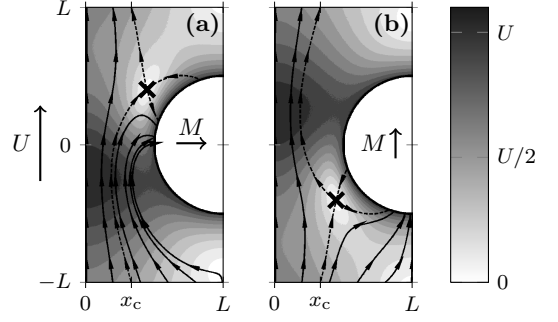


FIG. 2. Example particle trajectories (black curves) through a single periodic cell of the cylinder array and dimensionless particle speed (gray shading) as a function of position for dimensionless cylinder radius $d/R = 1$ and $\text{Mn} = 1$: (a) Setup A, (b) Setup B. The cross (\times) indicates the critical point between escape and capture. This point is a stationary point that is unstable to lateral perturbations. The dashed trajectories indicate the critical trajectories starting and ending in the critical point. The value x_c denotes the critical initial x -position between capture and escape at the inlet to the periodic cell.

for Setup A and B, respectively. Here the velocity scale, U , is taken as the maximum fluid velocity, occurring at the origin, *i.e.*, at the midpoint between neighboring cylinders.

We solve the flow problem of periodic Stokes flow through an infinite, regular cylinder array numerically with the Finite Element Method in FreeFEM++ for a range of cylinder radii and spacings.²³ Using this fluid velocity and approximating the magnetic field of an infinite cylinder array by that of a sufficiently large finite array (in practice a 10×19 array is sufficient), we can compute the particle velocity for any particle position and thus numerically integrate the particle trajectory from any given initial position (Fig. 2). In the case of a moderate cylinder magnetization, the particle can escape if it starts close enough to the midline between two cylinders. Along these trajectories, the magnetic force on the particle is too weak to overcome the viscous drag force. Since both the fluid flow and the magnetic force are periodic in y , these trajectories have to be periodic and so a particle that escapes one periodic cell of the cylinder array will also escape all subsequent cells.¹⁸

If a particle enters the cell closer to the cylinder, the stronger magnetic force and lower drag force due to slower fluid speeds closer to the cylinder wall both result in a trajectory that is more strongly influenced by the magnetic field. In Setup A, the particle is repelled from the front of the cylinder and attracted to its side where it is eventually captured (Fig. 2(a)). In Setup B, the particle is instead attracted to, and captured at, the front of the cylinder (Fig. 2(b)).

At the critical point, where the trajectories diverge between escape and capture, a particle would have zero speed, as indicated by the white background in Fig. 2.

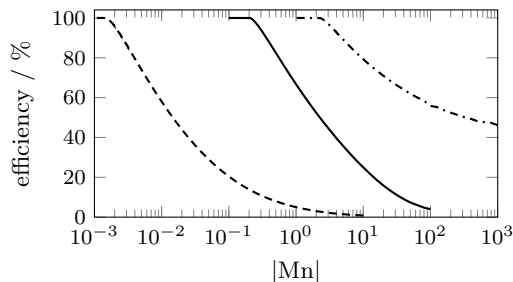


FIG. 3. Influence of the Mason number on the capture efficiency, $1 - x_c/L$, for different geometries: $d/R = 9$ (dashed), $d/R = 1$ (solid), $d/R = 1/9$ (dashdotted).

This stationary point is unstable with respect to lateral displacements. Comparing the two setups, the position of this critical point is mirrored along the x -axis. As the absolute value of the Mason number is decreased, the critical point moves from the cylinder wall to the y -axis.

We denote by x_c the critical initial x -position, *i.e.*, the initial x -position of the critical trajectory that leads from the inlet to the cell to the critical point. Particles with initial position $x < x_c$ will escape, those with $x \geq x_c$ will get captured.²⁴ Surprisingly, the value of x_c only depends on the absolute value of the Mason number, despite the very dissimilar limiting trajectories for positive and negative Mason numbers (Fig. 2). Assuming the filtrate is well mixed, the capture efficiency is given by $100(1 - x_c/L)\%$ and only depends on the absolute value of the Mason number and the geometry (Fig. 3).

For each geometry, there exists a critical absolute Mason number, Mn_{crit} , below which no particle can escape, regardless of its initial position at the inlet to the cell, and all particles are instead captured at the side or front of the cylinder depending on the setup (Fig. 3). The particle whose initial position lies on the midline between the two cylinders, *i.e.*, $(x_p(0), y_p(0)) = (0, -L)$, is the particle that is most easily able to escape, and will thus determine the critical Mason number. Due to symmetry, both the magnetic force and the fluid velocity have only components in the y -direction along this line and a particle that originates at $(0, -L)$ will, in theory, remain on the y -axis for all time. Thus, to find the critical Mason number, we may restrict our focus to the one-dimensional problem of whether or not a particle travelling along the y -axis escapes. In practice, instabilities or diffusion might move the particle away from the y -axis, so that it is captured even at higher Mason numbers, but the one-dimensional problem considered here provides an upper bound for the critical Mason number.

For Mason numbers with absolute value below the critical Mason number, the critical point lies on the y -axis and the particle velocity is negative along parts of this axis. For values above the critical Mason number, the particle velocity needs to be positive along the whole y -axis for the particle to be able to escape. Thus the critical Mason number is that absolute Mason num-

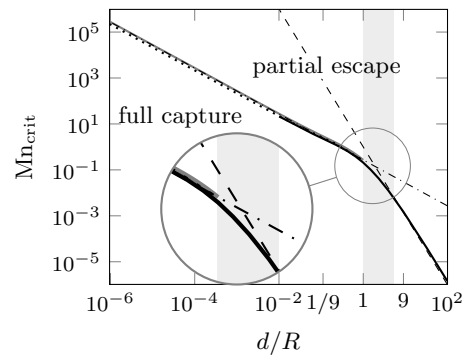


FIG. 4. Critical Mason number for different ratios of cylinder radius and spacing: numerical computation using the finite element flow field and the magnetic force from a cylinder array (thick solid), numerical computation using the lubrication flow field and the magnetic force from a cylinder array (thick dotted), numerical computation using the lubrication flow field and the magnetic force from only two cylinders (thick gray), asymptotic limit for small distances using the lubrication flow field and the magnetic force from only two cylinders (dash-dotted), asymptotic behavior for large distances (dashed). The shading indicates the parameter range representative of typical HGMS systems.^{9,16}

ber for which the particle velocity on the y -axis just reaches the value zero at some position.²¹ The capture efficiency and thus the critical Mason number depend on the geometry, namely the ratio d/R of the smallest distance between cylinders to the cylinder diameter (Fig. 3), which is related to the filter volume fraction, ϕ , by $d/R = \sqrt{\pi/(4\phi)} - 1$.

If the distances between cylinders are very small compared to their radii, that is $d/R \ll 1$, the flow field in the gap between two cylinders can be approximated by lubrication theory.²⁵ In addition, since all other cylinders are further away and thus contribute less to the overall magnetic force, we consider only the influence of these two cylinders on the magnetic field as a first approximation. Hence, we obtain the following asymptotic approximation for the critical Mason number²¹

$$Mn_{crit} = \frac{1}{216} (34\sqrt{2} + 5\sqrt{5}) \frac{R}{d} \approx 0.27 \left(\frac{d}{R}\right)^{-1} \quad (4)$$

as $d/R \rightarrow 0$.

For distant cylinders, such that $d/R \gg 1$, the velocity away from the cylinders along the y -axis is approximately constant, while the magnetic force along the y -axis decreases as

$$F_{m,y}(0, y) \sim \left(\frac{\sqrt{(d+R)^2 + y^2}}{R}\right)^{-3} \sim \mathcal{O}\left(\frac{d}{R}\right)^{-3} \quad (5)$$

as $d/R \rightarrow \infty$. Thus, we obtain $Mn_{crit} \sim \mathcal{O}(d/R)^{-3}$ in this limit.²¹

For cylinder separations that are of the same order of magnitude as the cylinder radius, that is $d/R = \mathcal{O}(1)$,

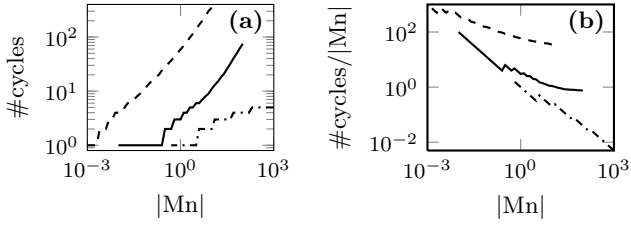


FIG. 5. Conditions on (a) number of cycles, (b) separation time, $t_{\text{sep}} \propto \text{\#cycles}/|\text{Mn}|$, to ensure 95% capture efficiency for different Mason numbers and different geometries: $d/R = 9$ (dashed), $d/R = 1$ (solid), $d/R = 1/9$ (dashdotted).

numerical solutions of the fluid flow field must be used (here obtained with the Finite Element package FreeFEM++).²³ The critical Mason numbers obtained via numerical solutions are in excellent agreement with the asymptotic limits (Fig. 4). If the setup is chosen such that the absolute value of the Mason number is below the critical Mason number then capture of all particles sent through the system can be guaranteed. To lower the Mason number to achieve this, one can, for example, reduce the fluid velocity through the cylinder array. Alternatively, our results imply that closer packing of the filter material improves capture efficiency by increasing the critical Mason number (Fig. 4). However, these improvements need to be weighed against the drop in flow rate and the concomitant reduced rate of production of clean water that this implies or the necessary increase in the pressure gradient to keep the flow rate the same.

If full capture is required, the system must operate below the critical Mason number. If, however, the required capture efficiency is lower, say only 95%, then for any given geometry and Mason number, it is possible to achieve this by repeating the separation several times, which may be faster than doing a single cycle at a lower Mason number. Before each separation cycle we assume that the suspension is mixed again to randomize the initial x -position of the particles. The separation cycles are then independent and we can infer how many cycles are necessary from the capture efficiency of a single separation cycle (Fig. 5(a)).

Since the absolute value of the Mason number depends linearly on the flow velocity, (3), doubling the flow rate through the system doubles the Mason number. Hence this increases the number of cycles necessary to achieve a required capture efficiency, but also halves the time each separation cycle lasts. Thus by dividing the number of necessary cycles by the absolute value of the Mason number, we can infer the effect of changing the Mason number on the total separation time, $t_{\text{sep}} \propto \text{\#cycles}/|\text{Mn}|$, neglecting any additional time that might be necessary between cycles (Fig. 5(b)). It is clearly inefficient to run the system below the highest Mason number that achieves the required capture efficiency or just above a Mason number at which the required number of cycles increases by one. Furthermore, our data suggests that it

would be overall more efficient to increase the flow rate and adapt the number of cycles accordingly. However, there are some caveats that must be considered. Firstly, a higher flow rate requires higher pressure gradients, which in turn implies a higher energy consumption. Secondly, we have not included any time for the tasks that may be necessary between separation cycles, such as re-mixing the solution. Lastly, in many industrial HGMS systems, the filter material is randomly packed rather than periodic. In this case, unlike in our setups, particles that escape the first wires in a filter may well be captured further downstream. Thus, the increasing number of cycles necessary to achieve a required capture efficiency at higher Mason numbers would then simply translate to increasing the length of the filter.

We have demonstrated two potential methods that guarantee a certain required particle capture efficiency in a periodic model of high gradient magnetic separation. We have computed the critical Mason number, below which full particle capture can be ensured, numerically and asymptotically, and shown how this depends on the filter geometrical parameter d/R . If the required capture efficiency is below 100%, then this can be achieved by repeating the separation process several times at $\text{Mn} > \text{Mn}_{\text{crit}}$. We have shown how the number of necessary cycles depends on the Mason number and the geometry and that it may be overall more efficient to carry out multiple separation cycles at a higher flow rate. The results of this work should be useful in advancing strategies for the removal of magnetic or paramagnetic particles.

This publication was based on work supported in part by Award No KUK-C1-013-04, made by King Abdullah University of Science and Technology (KAUST) and by Award No 113/277 made by the John Fell Fund.

- ¹Cafer T. Yavuz, Arjun Prakash, J. T. Mayo, and Vicki L. Colvin. Magnetic separations: From steel plants to biotechnology. *Chem. Eng. Sci.*, 64:2510–2521, 2009.
- ²Ritu D. Ambashta and Mika Sillanpää. Water purification using magnetic assistance: A review. *J. Hazard. Mater.*, 180(1–3):33–49, August 2010.
- ³S. Hayashi, F. Mishima, Y. Akiyama, and S. Nishijima. Development of superconducting high gradient magnetic separation system for highly viscous fluid for practical use. *Physica C*, 471(2122):1511–1515, 2011. The 23rd International Symposium on Superconductivity.
- ⁴Ashok Sinha, Ranjan Ganguly, Anindya K. De, and Ishwar K. Puri. Single magnetic particle dynamics in a microchannel. *Phys. Fluids*, 19(11):117102, 2007.
- ⁵S. S. H. Tsai, I. M. Griffiths, and H. A. Stone. Microfluidic immunomagnetic multi-target sorting – a model for controlling deflection of paramagnetic beads. *Lab Chip*, 11:2577–2582, 2011.
- ⁶Metso Corporation. *High gradient magnetic separators: HGMS cyclic*. Technical specification: TS HGMS cyclic 1105-en.
- ⁷H. Pfister. Magnetische Separation mit hohen Flusssdichtegradienten. *J. Magn. Magn. Mater.*, 13(1–2):1–10, Sep 1979.
- ⁸Richard Gerber and Robert R. Birss. *High gradient magnetic separation*. Electronic & electrical engineering research studies. Magnetic materials and their applications series. Research Studies Press, 1983.
- ⁹Daniel L. Cummings, David A. Himmelblau, John A. Oberteuffer, and Gary J. Powers. Capture of small paramagnetic parti-

- cles by magnetic forces from low speed fluid flows. *AIChE J.*, 22(3):569575, 1976.
- ¹⁰Armin D. Ebner and James A. Ritter. New correlation for the capture cross section in high-gradient magnetic separation. *AIChE J.*, 47(2):303313, 2001.
- ¹¹F. Mishima, S. Hayashi, Y. Akiyama, and S. Nishijima. Development of a superconducting high gradient magnetic separator for a highly viscous fluid. *IEEE Trans. Appl. Superconduct.*, 22(3):3700204–3700204, June 2012.
- ¹²S. Uchiyama, S. Kurinobu, M. Kumazawa, and M. Takayasu. Magnetic particle buildup processes in parallel stream type hgms filter. *IEEE Trans. Magn.*, 13(5):1490–1492, Sep 1977.
- ¹³Fei Chen, Kenneth A. Smith, and T. Alan Hatton. A dynamic buildup growth model for magnetic particle accumulation on single wires in high-gradient magnetic separation. *AIChE J.*, 58(9):2865–2874, 2012.
- ¹⁴Johannes Lindner, Katharina Menzel, and Hermann Nirschl. Simulation of magnetic suspensions for HGMS using CFD, FEM and DEM modeling. *Comput. Chem. Eng.*, 54:111 – 121, 2013.
- ¹⁵C. O. Too, M. R. Parker, R. Gerber, and D. Fletcher. Optimisation of matrix design in high gradient magnetic separation. *J. Phys. D: Appl. Phys.*, 19(1):L1, 1986.
- ¹⁶Y. G. Kim, J. B. Song, D. G. Yang, J. S. Lee, Y. J. Park, D. H. Kang, and H. G. Lee. Effects of filter shapes on the capture efficiency of a superconducting high-gradient magnetic separation system. *Supercond. Sci. Technol.*, 26(8):085002, 2013.
- ¹⁷K. Hayashi and S. Uchiyama. On particle trajectory and capture efficiency around many wires. *IEEE Trans. Magn.*, 16(5):827–829, 1980.
- ¹⁸William H. Simons and Richard P. Treat. Particle trajectories in a lattice of parallel magnetized fibers. *J. Appl. Phys.*, 51(1):578, 1980.
- ¹⁹Giacomo Mariani, Massimo Fabbri, Francesco Negrini, and Pier Luigi Ribani. High-gradient magnetic separation of pollutant from wastewaters using permanent magnets. *Sep. Purif. Technol.*, 72(2):147 – 155, 2010.
- ²⁰C. T. Yavuz, J. T. Mayo, W. W. Yu, and A. Prakash. Low-field magnetic separation of monodisperse Fe_3O_4 nanocrystals. *Science*, 314:964–967, 2006.
- ²¹See attached supplementary material for details of the computation of the critical Mason number and its asymptotic approximations.
- ²²Tae Gon Kang, Martien A. Hulsen, and Jaap M. J. den Toonder. Dynamics of magnetic chains in a shear flow under the influence of a uniform magnetic field. *Phys. Fluids*, 24:042001, 2012.
- ²³F. Hecht. *FreeFem++*, third edition, April 2014. Version 3.30.
- ²⁴Due to our choice of coordinate system, the “capture distance” or “capture cross section” from the literature^{9,18} is $L - x_c$.
- ²⁵H. Ockendon and J. R. Ockendon. *Viscous flow*. Cambridge University Press, 1995.

Supplementary material

I. PROBLEM DESCRIPTION

We consider a single spherical magnetic particle moving through an infinite square array of infinitely long parallel cylinders of radius R with a constant magnetization perpendicular to their axes. The particle is carried by a fluid flow and deflected by the magnetic force exerted due to the magnetic field of the cylinders (Fig. 1). We study two different setups. In Setup A, the magnetization of the cylinders and the particle are perpendicular to the flow direction (Fig. 1). In Setup B, both magnetizations are parallel to the flow direction. The flow is assumed to be planar, steady, periodic Stokes flow through the array.

II. MAGNETIC FORCE ON PARTICLE AROUND A SINGLE CYLINDER

We approximate the magnetic force on the particle in the infinite cylinder array by adding the contributions of single cylinders in a sufficiently large finite array. First consider setup A.

The magnetic field, \mathbf{B} , induced by a single infinitely long cylinder with radius R and uniform magnetization, $\mathbf{M} = M\mathbf{e}_x$, perpendicular to its axis is^{1,2} (Fig. 6a)

$$\begin{aligned} \mathbf{B}_{\text{single}}(r, \theta) &= \frac{\mu_0 M}{2} \left(\frac{R}{r} \right)^2 [\cos \theta \mathbf{e}_r + \sin \theta \mathbf{e}_\theta] \\ &= \frac{\mu_0 M}{2} \left(\frac{R}{r} \right)^2 [\cos 2\theta \mathbf{e}_x + \sin 2\theta \mathbf{e}_y], \end{aligned} \quad (6)$$

outside of the cylinder, where μ_0 is the permeability of free space, r and θ are the plane-polar coordinates centered on the cylinder and \mathbf{e}_x , \mathbf{e}_y and \mathbf{e}_r , \mathbf{e}_θ are the unit vectors in Cartesian and plane-polar coordinates, respectively (see Fig. 7).

We place into this field a spherical paramagnetic particle. If this particle is uniformly magnetized then it behaves precisely like a dipole of moment \mathbf{m} . The force on a magnetic dipole \mathbf{m} in a given magnetic field \mathbf{B} is given by³

$$\mathbf{F}_m = \nabla (\mathbf{m} \cdot \mathbf{B}). \quad (7)$$

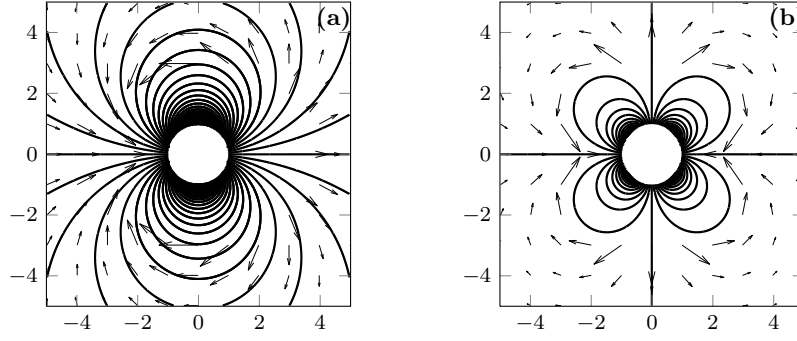


FIG. 6. (a) The magnetic field, \mathbf{B} , around a cylinder with uniform magnetization, $\mathbf{M} = M\mathbf{e}_x$, perpendicular to its axis. (b) The magnetic force, \mathbf{F} , on a particle around this cylinder with its magnetic dipole moment, $\mathbf{m} = m\mathbf{e}_x$, aligned to the cylinder magnetization.

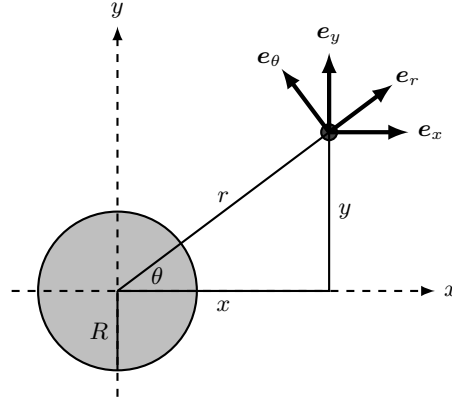


FIG. 7. Coordinate systems for single cylinder.

Since the sphere is paramagnetic, its dipole moment is aligned with the surrounding magnetic field. We assume that the magnetic field of the cylinder is just a small perturbation of a stronger uniform outer field, aligned with the cylinder magnetization, *i.e.*,

$$\mathbf{m} = m\mathbf{e}_x. \quad (8)$$

A uniform field does not create a force on the dipole, thus, using the magnetic field (6), we obtain (Fig. 6b)

$$\begin{aligned} \mathbf{F}_{\text{m, single}} &= \nabla (\mathbf{m} \cdot \mathbf{B}) = \frac{\mu_0 m M R^2}{2} \nabla \left(\frac{\cos 2\theta}{r^2} \right) = -\frac{\mu_0 m M R^2}{r^3} (\cos 2\theta \mathbf{e}_r + \sin 2\theta \mathbf{e}_\theta) \\ &= -\frac{\mu_0 m M R^2}{r^3} (\cos 3\theta \mathbf{e}_x + \sin 3\theta \mathbf{e}_y). \end{aligned} \quad (9)$$

In setup B, the magnetization of the cylinder and the magnetic dipole moment of the particle are rotated by $\pi/2$ and aligned with the y -axis, *i.e.*, $\mathbf{M} = M\mathbf{e}_y$ and $\mathbf{m} = m\mathbf{e}_y$. In this case, the sign of the force swaps (compare Fig. 6b). Thus, we can express both setups in one formula as

$$\mathbf{F}_{\text{m, single}} = \mp \frac{\mu_0 m M}{R} \left(\frac{R}{r} \right)^3 \begin{pmatrix} \cos 3\theta \\ \sin 3\theta \end{pmatrix}. \quad (10)$$

III. NONDIMENSIONALIZATION AND MASON NUMBER

Neglecting inertial terms, the net force on the particle must be zero, *i.e.*, the magnetic force, \mathbf{F}_m , and the viscous drag force (Stokes drag) due to the flow field, \mathbf{u} , must balance, giving an ODE for the particle trajectory, $\mathbf{x}_p(t)$,

$$6\pi\eta a \left(\mathbf{u}(\mathbf{x}_p) - \frac{\partial \mathbf{x}_p}{\partial t} \right) + \mathbf{F}_m = 0, \quad (11)$$

with η the fluid viscosity and a the particle radius.

Scaling the velocities with the maximum fluid velocity, U , and the magnetic force with $\mu_0 m M / R$, *i.e.*, the maximum magnetic force a single cylinder could exert on the particle, and choosing a suitable length scale \sqrt{Rd} for the geometry of the cylinder array we get

$$x = \sqrt{Rd}\hat{x}, \quad y = \sqrt{Rd}\hat{y}, \quad \mathbf{x}_p = \sqrt{Rd}\hat{\mathbf{x}}_p, \quad \mathbf{u} = U\hat{\mathbf{u}}, \quad t = \frac{\sqrt{Rd}}{U}\hat{t}, \quad \mathbf{F}_m = \pm \frac{\mu_0 m M}{R} \hat{\mathbf{F}}_m. \quad (12)$$

Thus the force balance can be rewritten in dimensionless terms as

$$\frac{\partial \hat{\mathbf{x}}_p}{\partial \hat{t}} = \hat{\mathbf{u}} + \frac{1}{\text{Mn}} \hat{\mathbf{F}}_m \quad (13)$$

with the Mason number⁴

$$\text{Mn} = \pm \frac{|\mathbf{F}_v|}{|\mathbf{F}_m|} = \pm \frac{6\pi\eta a R U}{\mu_0 m M}. \quad (14)$$

The sign in the Mason number allows us to easily distinguish between setups A and B, while using the same dimensionless magnetic force, $\hat{\mathbf{F}}_m$.

IV. CRITICAL MASON NUMBER IN INFINITE SQUARE CYLINDER ARRAY

Due to symmetry, along a midline between two columns of cylinders, *e.g.*, at $\hat{x} = 0$, both the dimensionless magnetic force and the dimensionless fluid velocity only have components in the \hat{y} -direction. Thus, we can consider them as functions of \hat{y} only, say $\hat{F}_{\hat{y}}(\hat{y})$ and $\hat{v}(\hat{y})$, respectively, and a particle on the midline will in theory remain there for all time. If this particle escapes, its velocity, $\partial \hat{\mathbf{x}}_p / \partial \hat{t} = \hat{v}(\hat{y}) + \hat{F}_{\hat{y}} / \text{Mn}$, is always positive. If it cannot escape, this means that $\partial \hat{\mathbf{x}}_p / \partial \hat{t} \leq 0$ along part of the \hat{y} -axis. At the critical Mason number, there just about exists a stationary point on the \hat{y} -axis, that is

$$\exists \hat{y}^* : \quad 0 = \hat{v}(\hat{y}^*) + \frac{1}{\text{Mn}} \hat{F}_{\hat{y}}(\hat{y}^*), \quad \text{while} \quad 0 \leq \hat{v}(\hat{y}) + \frac{1}{\text{Mn}} \hat{F}_{\hat{y}}(\hat{y}) \quad \forall \hat{y}, \quad (15)$$

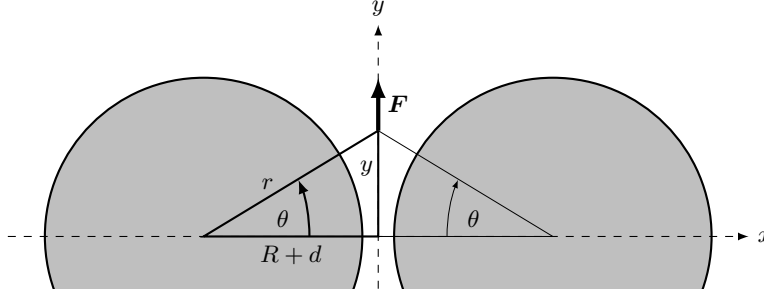
or

$$\exists \hat{y}^* : \quad |\text{Mn}| = \mp \frac{\hat{F}_{\hat{y}}(\hat{y}^*)}{\hat{v}(\hat{y}^*)} \quad \text{and} \quad |\text{Mn}| \geq \mp \frac{\hat{F}_{\hat{y}}(\hat{y})}{\hat{v}(\hat{y})} \quad \forall \hat{y}. \quad (16)$$

Since $\hat{F}_{\hat{y}}(\hat{y})$ and $\hat{v}(\hat{y})$ are odd and even functions respectively, this absolute value of the Mason number is independent of the sign, and so does not depend on the setup. Hence, we define the critical Mason number as

$$\text{Mn}_{\text{crit}} := |\text{Mn}| = \max_{\hat{y}} \left(\mp \frac{\hat{F}_{\hat{y}}(\hat{y})}{\hat{v}(\hat{y})} \right). \quad (17)$$

If $|\text{Mn}| \leq \text{Mn}_{\text{crit}}$ then we can guarantee full capture; if $|\text{Mn}| > \text{Mn}_{\text{crit}}$ then some particles will escape the cylinder array.

FIG. 8. Geometry along the y -axis.

V. DERIVATION OF THE ASYMPTOTIC CRITICAL MASON NUMBER FROM LUBRICATION THEORY

The flow through two very close cylinders can be approximated using lubrication theory⁵. With R the cylinder radius and $2d$ the minimum cylinder gap thickness, the width of the gap along the y -axis is $2h$, with

$$h(y) = d + R - \sqrt{R^2 - y^2} \sim \left(1 + \frac{y^2}{2Rd}\right) d + \mathcal{O}(y^3). \quad (18)$$

In x -direction, we nondimensionalize with d . Since the gap width, $2h$, varies on the scale \sqrt{Rd} , we use this scale to nondimensionalize y . Upon nondimensionalizing Stokes equations with

$$x = d\hat{x}, \quad y = \sqrt{Rd}\hat{y}, \quad u = \sqrt{\frac{d}{R}}U\hat{u}, \quad v = U\hat{v}, \quad (19)$$

$$h(y) \sim d\hat{h}(\hat{y}) = d\left(1 + \frac{\hat{y}^2}{2}\right), \quad p = p_0 + \frac{\eta U \sqrt{R}}{d^{3/2}}\hat{p}, \quad (20)$$

we obtain at leading order

$$0 = -\frac{\partial \hat{p}}{\partial \hat{x}}, \quad 0 = -\frac{\partial \hat{p}}{\partial \hat{y}} + \frac{\partial^2 \hat{v}}{\partial \hat{x}^2}, \quad 0 = \frac{\partial \hat{u}}{\partial \hat{x}} + \frac{\partial \hat{v}}{\partial \hat{y}}, \quad (21)$$

with boundary conditions

$$\hat{u} = 0, \quad \hat{v} = 0 \quad \text{at} \quad \hat{x} = \hat{h}(\hat{y}), \quad \hat{u} = 0, \quad \frac{\partial \hat{v}}{\partial \hat{x}} = 0 \quad \text{at} \quad \hat{x} = 0. \quad (22)$$

This can be solved by integrating across the thickness to obtain

$$\hat{u}(\hat{x}, \hat{y}) = \hat{h}' \left[\frac{\hat{x}}{\hat{h}^2} - \frac{\hat{x}^3}{\hat{h}^4} \right], \quad \hat{v}(\hat{x}, \hat{y}) = \frac{1}{\hat{h}^3} \left[\hat{h}^2 - \hat{x}^2 \right], \quad \frac{d\hat{p}}{d\hat{y}} = -\frac{2}{\hat{h}^3}, \quad (23)$$

where $\hat{h} = \hat{h}(\hat{y})$ and the prime denotes differentiation.

Following equation (17), it is only the midline that concerns us here, *i.e.*, (Fig. 8)

$$x = 0, \quad y = (R + d) \tan \theta, \quad r = \frac{R + d}{\cos \theta}, \quad (24)$$

thus

$$\hat{x} = 0, \quad \hat{y} = \left(\sqrt{\frac{R}{d}} + \sqrt{\frac{d}{R}} \right) \tan \theta, \quad \hat{r} = \frac{r}{R} = \frac{1 + d/R}{\cos \theta}, \quad (25)$$

so that the vertical fluid velocity from (23) is

$$\hat{v}(\theta) = \frac{1}{\hat{h}} = \frac{1}{1 + \frac{\hat{y}^2}{2}} = \left(1 + \frac{1}{2} \left(\sqrt{\frac{R}{d}} + \sqrt{\frac{d}{R}} \right)^2 \tan^2 \theta \right)^{-1} \quad (26)$$

and, considering only these two cylinders, the \hat{y} -component of the magnetic force is

$$\hat{F}_{\hat{y}}(\theta) = -\frac{2}{(1+d/R)^3} \cos^3 \theta \sin 3\theta. \quad (27)$$

Let

$$g(\theta) = -\frac{\hat{F}_{\hat{y}}(\theta)}{\hat{v}(\theta)}, \quad (28)$$

then

$$\text{Mn}_{\text{crit}} = \max_{\theta \in (-\frac{\pi}{2}, \frac{\pi}{2})} g(\theta). \quad (29)$$

Hence

$$\begin{aligned} g(\theta) &= \frac{2}{(1+d/R)^3} \cos^3 \theta \sin 3\theta \left(1 + \frac{1}{2} \left(\sqrt{\frac{R}{d}} + \sqrt{\frac{d}{R}} \right)^2 \tan^2 \theta \right) \\ &= \frac{2}{(1+d/R)^3} \cos^3 \theta \sin 3\theta + \frac{1}{(1+d/R)(d/R)} \cos \theta \sin^2 \theta \sin 3\theta. \end{aligned} \quad (30)$$

However, we can improve our understanding, by noting that for $d/R \rightarrow 0$, $2/(1+d/R)^3 \rightarrow 2$, whereas $1/((1+d/R)(d/R)) \sim (d/R)^{-1}$, so that

$$g(\theta) \sim \left(\frac{d}{R} \right)^{-1} \tilde{g}(\theta) = \left(\frac{d}{R} \right)^{-1} \cos \theta \sin^2 \theta \sin 3\theta \quad (31)$$

and hence

$$\begin{aligned} g'(\theta) &\sim \left(\frac{d}{R} \right)^{-1} \tilde{g}'(\theta) = \left(\frac{d}{R} \right)^{-1} [-\sin^3 \theta \sin 3\theta + 2 \cos^2 \theta \sin \theta \sin 3\theta \\ &\quad + 3 \cos \theta \cos 3\theta \sin^2 \theta] \\ &= \left(\frac{d}{R} \right)^{-1} \sin^2 \theta [2 + 4 \cos 2\theta + 3 \cos 4\theta] \\ &= \left(\frac{d}{R} \right)^{-1} \sin^2 \theta [24 \cos^4 \theta - 16 \cos^2 \theta + 1]. \end{aligned} \quad (32)$$

A maximum of $g(\theta)$ has $g'(\theta^*) = 0$ and so either $\theta^* = 0$ (not a max.) or

$$24 \cos^4 \theta^* - 16 \cos^2 \theta^* + 1 = 0. \quad (33)$$

Thus follows that for d/R small enough,

$$\text{Mn}_{\text{crit}} = \max_{\theta} g(\theta) = g(\theta^*) \sim \frac{1}{216} (34\sqrt{2} + 5\sqrt{5}) \left(\frac{d}{R} \right)^{-1} \approx 0.2744 \left(\frac{d}{R} \right)^{-1}. \quad (34)$$

¹Richard Gerber and Robert R. Birss. *High gradient magnetic separation*. Electronic & electrical engineering research studies. Magnetic materials and their applications series. Research Studies Press, 1983.

²Julius Adams Stratton. *Electromagnetic theory*. McGraw-Hill Book Company, 1941.

³David Jeffrey Griffiths. *Introduction to electrodynamics*. Prentice Hall, third edition, 1999.

⁴Tae Gon Kang, Martien A. Hulsen, and Jaap M. J. den Toonder. Dynamics of magnetic chains in a shear flow under the influence of a uniform magnetic field. *Phys. Fluids*, 24:042001, 2012.

⁵H. Ockendon and J. R. Ockendon. *Viscous flow*. Cambridge University Press, 1995.